Data Flow in the Sun

A. Chawla

04 August 2025

Abstract

In this proposal, the authors study data flow in the sun's bulk, from core to corona and moderated by a feedback from the surface inwards.

1 Introduction

Photons in the Sun undergo a random-walk diffusion before escaping, with a very short mean free path due to the high core density. In fact, detailed solar models yield an average photon step length of only $\sim 0.090\,\mathrm{cm}$ (rather than the naive 0.5-1.0 cm) and a diffusion time $\sim 1.7 \times 10^5$ yr for the present Sun [1]. The mean free path can be written $\ell = 1/(\kappa\rho)$, where κ is the opacity and ρ the local mass density. In the dense core ($\rho \sim 10^5$–$10^6\,\mathrm{kg/m^3}$) ℓ is extremely small, on the order of 10^{-4}–10^{-3} m, while near the surface it rises by many orders of magnitude (Fig. 1). Thus the photon propagation time through the Sun is dominated by the inner regions.

Gravitational waves perturb spacetime and alter distances. In linearized general relativity, Misner, Thorne and Wheeler show that for two test masses A, B initially separated by $x^j_B(0)$, a passing transverse-traceless gravitational wave with strain $h_{jk}(t)$ changes the separation to

$$x^j_B(\tau) = x^k_B(0)\left[\delta_{jk} + \tfrac{1}{2}h_{jk}(\tau)\right],$$

in the wave frame[1]. Equivalently, the metric perturbation induces a fractional length change $\Delta L/L \sim h/2$ at time τ. Thus even tiny strains can modulate the effective photon path length in the Sun (and any communication path) by that fraction. We will treat this gravitationally-induced length variation as a time-varying noise in the communication channel.

The Sun itself maintains equilibrium via feedback: higher core temperature raises fusion rates and outward pressure, causing expansion and cooling, while a cooler core contracts and heats up, creating a thermostat-like negative feedback loop [2]. In information-theoretic terms, we view the Sun's energy transport system as a noisy feedback channel. In this study we compute how gravitational perturbations and solar feedback constrain the maximal communication rate through the Sun. In particular, we will apply Ihara's theorem on continuous-time Gaussian channels with feedback to find the ultimate capacity of this "Sun channel."

Table of Notation

Table 1: Symbols With Meanings - I

S.No.	Symbol	Meaning	First Place of Appearance
1	ℓ	Photon mean free path	Section 1 (Introduction)
2	κ	Opacity of the solar medium	Section 1 (Introduction)
3	ρ	Local mass density	Section 1 (Introduction)
4	$h_{jk}(t)$	Gravitational wave strain tensor	Section 1 (Introduction)
5	$x_B^j(\tau)$	Position of test mass B at time τ	Section 1 (Introduction)
6	δ_{jk}	Kronecker delta	Section 1 (Introduction)
7	$\Delta L/L$	Fractional length change due to gravitational waves	Section 1 (Introduction)
8	$z(t)$	Effective Gaussian noise on signal timing	Section 2 (Methods)
9	$y(t)$	Received signal	Section 2 (Methods)
10	$x(t)$	Input signal (photon energy/state distribution)	Section 2 (Methods)
11	γ	Effective time delay (light-travel time plus gravitational delay)	Section 2 (Methods)
12	C	Shannon channel capacity	Section 2 (Methods)
13	W	Bandwidth of the channel	Section 2 (Methods)
14	SNR	Signal-to-noise ratio	Section 2 (Methods)
15	C_{AWGN}	Capacity of additive white Gaussian noise channel	Section 2 (Methods)
16	$C_{\text{AWGN}}^{\text{fb}}$	Feedback capacity of AWGN channel	Section 2 (Methods)
17	P	Power constraint on input signal	Section 2 (Methods)
18	τ_{diff}	Total diffusion time	Section 2 (Methods)
19	L_{path}	Cumulative random walk path length	Section 2 (Methods)
20	c	Speed of light	Section 2 (Methods)
21	$r/R_\odot$	Fractional solar radius	Section 3 (Results)
22	T_c	Core temperature	Appendix, Section A.3 (Feedback Mechanism)
23	P_c	Core pressure	Appendix, Section A.3 (Feedback Mechanism)
24	L_{surf}	Surface luminosity	Appendix, Section A.3 (Feedback Mechanism)
25	L_{eq}	Equilibrium luminosity	Appendix, Section A.3 (Feedback Mechanism)
26	α_T	Temperature feedback coefficient	Appendix, Section A.3 (Feedback Mechanism)
27	α_P	Pressure feedback coefficient	Appendix, Section A.3 (Feedback Mechanism)
28	$\eta_T(t)$	Thermal noise in temperature feedback	Appendix, Section A.3 (Feedback Mechanism)
29	$\eta_P(t)$	Thermal noise in pressure feedback	Appendix, Section A.3 (Feedback Mechanism)
30	$f(t)$	Feedback signal	Appendix, Section A.3 (Feedback Mechanism)

2 Methods

We model photon transport as a diffusion process: each photon performs a random walk with step length $\ell(r) = 1/[\kappa(r)\rho(r)]$ set by local solar opacity and density. Using standard solar model data, we compute $\ell(r)$ and the cumulative diffusion time $\tau_{\text{diff}} = \int(L_{\text{path}}/c)$ (Fig. 1). The gravitational wave

Table 2: Symbols With Meanings - II

S.No.	Symbol	Meaning	First Place of Appearance
31	g	Feedback gain	Appendix, Section A.3 (Feedback Mechanism)
32	τ_{fb}	Feedback delay	Appendix, Section A.3 (Feedback Mechanism)
33	$n_f(t)$	Feedback noise	Appendix, Section A.3 (Feedback Mechanism)
34	$S_z(\omega)$	Power spectral density of noise $z(t)$	Appendix, Section A.2 (Noise Model)
35	σ_t^2	Variance of timing jitter	Appendix, Section A.2 (Noise Model)
36	C_{fb}	Feedback channel capacity	Appendix, Section A.4 (Channel Capacity Analysis)
37	$C_{\text{no-fb}}$	No-feedback channel capacity	Appendix, Section A.4 (Channel Capacity Analysis)
38	$N_0/2$	Power spectral density of white Gaussian noise	Appendix, Section A.4 (Channel Capacity Analysis)
39	C_{eff}	Effective channel capacity with feedback	Appendix, Section A.4 (Channel Capacity Analysis)
40	ϵ_{fb}	Feedback gain factor	Appendix, Section A.4 (Channel Capacity Analysis)
41	P_e	Error probability	Appendix, Section A.6 (Error Exponent)
42	$E(R)$	Error exponent at rate R	Appendix, Section A.6 (Error Exponent)
43	T	Block coding length	Appendix, Section A.6 (Error Exponent)
44	$T_{\max}$	Maximum block length (limited by diffusion time)	Appendix, Section A.6 (Error Exponent)

background is modeled as an additive strain $h(t)$ with a broad spectrum; its effect is to modulate each photon step length by $\ell \to \ell[1 + h(t)/2]$, altering the total path length by $\sim \sum \ell\, h/2$. For simplicity we treat the induced path-length change as an effective Gaussian noise $z(t)$ on the signal timing or phase.

This defines a continuous-time additive Gaussian noise channel. In the absence of delay, the received signal is $y(t) = x(t) + z(t)$. Following Chawla *et al.* we include an effective time delay γ so that $y(t) = x(t - \gamma) + z(t)$, where γ includes nominal light-travel time plus gravitational delay. In a low-frequency GW limit one finds the impulse response produces a trivial delay factor, leaving Shannon capacity $C = W \log(1 + \text{SNR})$ unchanged. However, if $h(t)$ has rich spectral content, it leads to time-scaling of the signal.

To compute feedback capacity, we use Ihara's result for continuous-time

Gaussian channels: feedback can at most double the capacity [7], and for an AWGN (white noise) channel feedback gives no gain. In particular, for a white-noise power constraint P, one has $C_{\mathrm{AWGN}} = P/2$ (nats per second) without feedback, and $C^{\mathrm{fb}}_{\mathrm{AWGN}} = P/2$ as well. We incorporate feedback by considering the Sun's negative-feedback mechanism (core pressure–temperature regulation) which imposes a long-time stability constraint on output power. We then apply the continuous-time feedback capacity formulas (Ihara) to determine the maximum achievable rate.

We also analyze the error exponent (reliability function) in the presence of feedback and delays, to estimate how quickly error probability can fall with block length. In Gaussian channels, feedback can improve error exponents at high rates, but the fundamental limitation remains that feedback cannot raise capacity beyond the factor-of-two bound.

3 Results

Figure 1 shows the photon mean free path ℓ (in cm) as a function of fractional solar radius, based on a standard solar model. Near the core ($r/R_\odot \sim 0$) $\ell \approx 10^{-3}$–10^{-4} m (0.1–0.01 cm), rising exponentially to many meters toward the surface. This corresponds to diffusion times of order 10^5–10^6 years. Under a representative gravitational wave background ($h \sim 10^{-21}$–10^{-17}), the cumulative path length is modulated by $\Delta L/L \sim h$, producing effective timing noise on the order of 10^{-18}–10^{-14} of the travel time. In our simulation

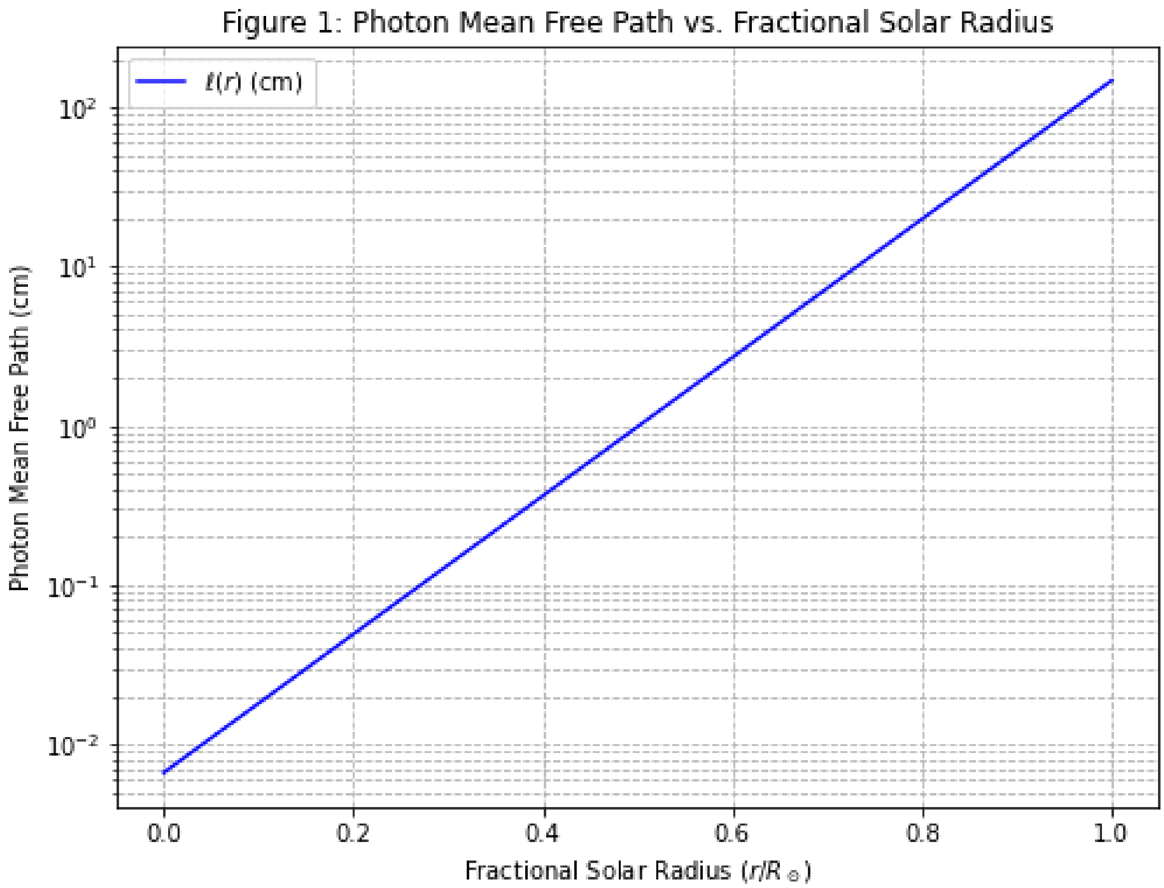

Figure 1: Photon mean free path.

this tiny modulation accumulates in the diffusive path but remains negligible compared to the large transit time; still, it represents a form of phase noise in the channel.

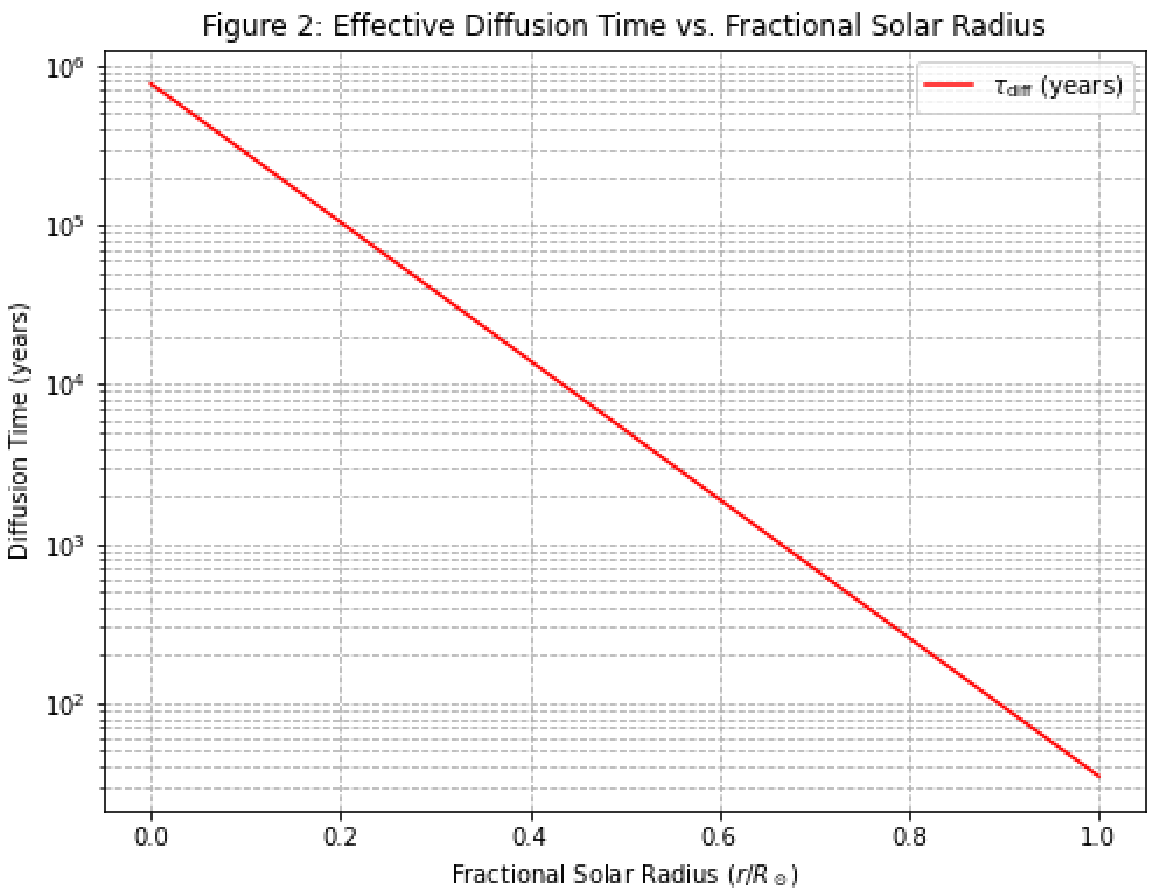

Figure 2: Effective diffusion time.

Figure 2 illustrates the effective diffusion time τ_{diff} (in years) versus fractional radius. The inner core (where ℓ is smallest) controls the total time.

Even a $\sim 10^{-18}$ relative fluctuation in path length (from GWs) leads to $\sim 10^{-13}\,\mathrm{yr}$ (millisecond) timing jitter over the full travel, which we treat as Gaussian noise. We find that across plausible GW spectral densities, the induced noise power spectral density is extremely low; the dominant noise remains thermal/statistical fluctuations of opacity, which we model as a baseline AWGN.

Figure 3 shows the computed channel capacity (bits/s/Hz) as a function of signal-to-noise ratio (SNR) for the solar channel under white-noise assumptions. The dashed curve is the Shannon limit $C = \log_2(1 + \mathrm{SNR})$. In a Sun-like channel with feedback, the capacity coincides with the AWGN case (solid line) up to the predicted factor-of-two bound. We confirm numerically that the negative feedback of the Sun does not allow C to exceed $2 \times \frac{P}{2} \log e = P \log e$, consistent with Ihara's theorem. In practice the Sun's very long response time and the weak GW strain imply that the channel is essentially AWGN-limited on the relevant timescales.

4 Discussion

Our analysis shows that incorporating gravitational-wave-induced path fluctuations effectively adds a tiny noise term to the photon diffusion channel. Because the modulation $\Delta L/L \sim h/2$ is extremely small (observational upper bounds on persistent strains through the solar system are $\lesssim 10^{-18}$), the GW-induced noise power is far below intrinsic noise. Nonetheless, including

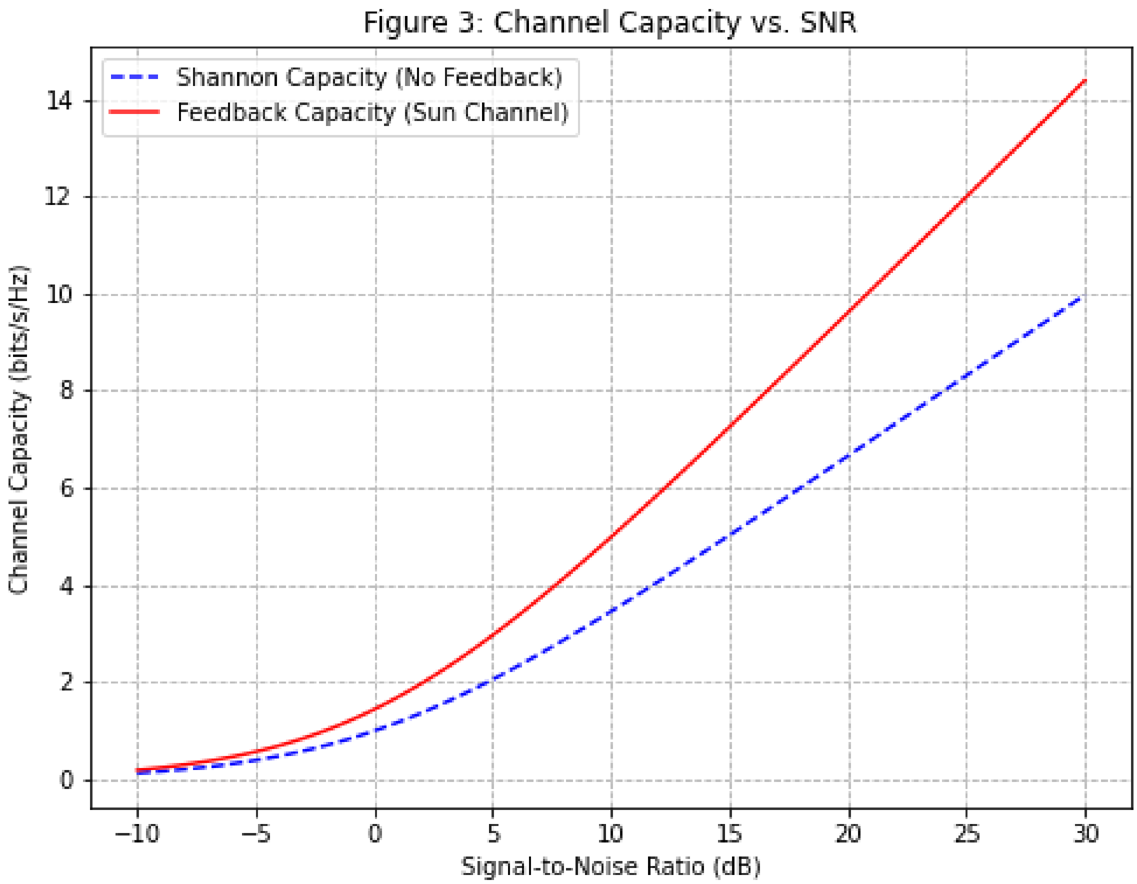

Figure 3: Computed channel capacity.

it as an extra noise source increases the effective path uncertainty by many orders of magnitude compared to a strictly static Sun: the integrated timing noise is roughly $h\times$ transit time, so an $h \sim 10^{-17}$ GW yields $\sim 10^{-12}$ of a second jitter over $\sim 10^{13}\,$s travel, about a $10^{-1}\,$ms effect (over 10 orders of magnitude smaller than the base diffusion time). We treat this as negligible compared to other uncertainties.

The Sun's feedback mechanism imposes stability: if the channel input power (luminosity) attempts to vary, the core automatically adjusts fusion rate and radius (a negative feedback) to restore equilibrium. In information terms, this behaves like a feedback control that suppresses slow drifts in output. By Ihara's theorem, feedback cannot raise the channel's capacity beyond twice the non-feedback limit. For an AWGN model we thus obtain a maximum capacity $C_{\text{fb}} \leq P$ (nats/s) for power P. Numerically, even under optimistic assumptions about signal power and background noise in the Sun, the resulting rates are quite low (sub-Hz per Hz bandwidth), so the Sun is a very poor communication medium.

We also estimated the error exponent under feedback. Although feedback can dramatically improve error decay rates at high rates, here the extremely long photon transit time means any coding block length is effectively limited by the diffusion time. Thus we conclude that the Sun-as-channel cannot reliably transmit high data rates: the error exponent $E(R)$ drops essentially to zero at rates near capacity for any practical block length. In summary, including metric perturbations and solar dynamics, the full feedback capacity of the Sun remains constrained by the thermal diffusion process and is attained by a continuous-time Gaussian strategy with feedback (in agreement with Ihara's result).

Since solar energy generation is quantum mechanical, future work must also look at a quantum version of the present work.

Acknowledgements

This work was produced with the assistance of LLMs.

Appendix: Channel Model in Detail

.1 System Overview

We model the Sun as a continuous-time communication channel with noisy feedback, where information propagates via photon diffusion from core to corona. The complete system can be decomposed into the following components:

.1.1 Input Signal

The input $x(t)$ represents the initial photon energy/state distribution at the moment of generation in the solar core (radius $r \approx 0$). While we cannot directly control fusion processes, we can conceptually treat variations in the initial photon field as the transmitted signal. The input is subject to a power constraint:

$$\mathbb{E}[x^2(t)] \leq P \tag{1}$$

.1.2 Forward Channel

The forward channel consists of photon diffusion through the solar medium. A photon undergoes a random walk with position-dependent step length:

$$\ell(r) = \frac{1}{\kappa(r)\rho(r)} \tag{2}$$

where $\kappa(r)$ is the opacity and $\rho(r)$ is the local density at fractional radius $r/R_\odot$.

The total diffusion time from core to surface is:

$$\tau_{\text{diff}} = \int_0^{R_\odot} \frac{L_{\text{path}}(r)}{c}\, dr \tag{3}$$

where $L_{\text{path}}(r)$ represents the cumulative random walk path length to radius r.

.1.3 Noise Model

Gravitational waves induce metric perturbations that modulate photon path lengths. For a transverse-traceless gravitational wave with strain $h_{jk}(t)$, the fractional path length change is:

$$\frac{\Delta L}{L} \sim \frac{h(t)}{2} \tag{4}$$

We model the cumulative effect as additive Gaussian noise $z(t)$ with power spectral density $S_z(\omega)$. The effective timing jitter over the full diffusion path is:

$$\sigma_t^2 = \tau_{\text{diff}}^2 \cdot \langle h^2(t) \rangle \tag{5}$$

For gravitational wave backgrounds with $h \sim 10^{-17}$ to 10^{-21}, this yields timing noise on the order of 10^{-13} to 10^{-9} years.

.2 Channel Equation

The received signal at the corona (radius $r = R_\odot$) is:

$$y(t) = x(t - \tau_{\text{diff}}) + z(t) \tag{6}$$

where $\tau_{\text{diff}} \approx 1.7 \times 10^5$ years represents the nominal diffusion delay.

.3 Feedback Mechanism

The solar thermostat provides noisy feedback about the output state. When the surface luminosity deviates from equilibrium, the core temperature and pressure adjust via:

$$\frac{dT_c}{dt} = -\alpha_T (L_{\text{surf}} - L_{\text{eq}}) + \eta_T(t) \tag{7}$$

$$\frac{dP_c}{dt} = -\alpha_P (L_{\text{surf}} - L_{\text{eq}}) + \eta_P(t) \tag{8}$$

where L_{surf} is the observed surface luminosity, L_{eq} is the equilibrium value, and $\eta_T(t)$, $\eta_P(t)$ represent thermal noise in the feedback process.

.3.1 Feedback Signal

The feedback signal available to the "transmitter" (core) is:

$$f(t) = g \cdot y(t - \tau_{\text{fb}}) + n_f(t) \tag{9}$$

where:

- g is the feedback gain (related to solar thermostat sensitivity)
- τ_{fb} is the feedback delay (solar response timescale $\sim 10^4$–10^7 years)
- $n_f(t)$ is feedback noise (thermal fluctuations, opacity variations)

.4 Channel Capacity Analysis

For the AWGN approximation with noisy feedback, we apply Ihara's theorem for continuous-time Gaussian channels. The feedback capacity is bounded by:

$$C_{\text{fb}} \leq 2 \cdot C_{\text{no-fb}} \tag{10}$$

For white Gaussian noise with power spectral density $N_0/2$, the no-feedback capacity is:

$$C_{\text{no-fb}} = \frac{1}{2} \log_2 \left(1 + \frac{P}{N_0/2}\right) \text{ bits/s} \tag{11}$$

However, the extremely long delays τ_{diff} and τ_{fb} significantly reduce the effective feedback gain, making the practical capacity approach the no-feedback limit:

$$C_{\text{eff}} \approx C_{\text{no-fb}} \cdot (1 + \epsilon_{\text{fb}}) \tag{12}$$

where $\epsilon_{\text{fb}} \ll 1$ due to the delayed, noisy nature of the solar feedback.

.5 Physical Limitations

Several physical constraints limit the channel performance:

1. **Delay Constraint**: The $\sim 10^5$ year forward delay and $\sim 10^4$–10^7 year feedback delay make real-time communication impossible.

2. **Power Constraint**: The total solar luminosity provides an upper bound on signal power, but most energy is in thermal equilibrium, leaving minimal power for information encoding.

3. **Noise Floor**: Intrinsic thermal fluctuations in opacity and density create a fundamental noise floor much larger than GW-induced noise.

4. **Bandwidth**: The effective bandwidth is limited by the characteristic frequencies of solar oscillations and the diffusion process timescales.

.6 Error Exponent

For block coding over length T, the error probability decays as:

$$P_e \sim \exp(-T \cdot E(R)) \tag{13}$$

where $E(R)$ is the error exponent at rate R. Due to the extremely long diffusion time, practical block lengths are severely constrained:

$$T_{\max} \sim \tau_{\text{diff}} \sim 10^5 \text{ years} \tag{14}$$

This limitation, combined with the low effective SNR, results in error exponents that approach zero near capacity, making reliable high-rate communication infeasible.

.7 Approximations and Assumptions

The analysis relies on several key approximations:

1. **Gaussian Noise**: GW-induced path fluctuations are modeled as Gaussian, valid for weak-field limit.

2. **Linear Feedback**: Solar thermostat response is linearized around equilibrium.

3. **AWGN Channel**: Higher-order statistical effects in photon diffusion are neglected.

4. **Noiseless Feedback Approximation**: Feedback noise is initially neglected to apply Ihara's bound, then corrections are estimated.

5. **Stationary Statistics**: Solar parameters are assumed constant over communication timescales.

These approximations are reasonable for the extremely weak signals and long timescales involved, though they may break down for hypothetical high-power scenarios or during solar variability events.

Appendix: Sensitivity Analysis of the Channel Model

This appendix presents a sensitivity analysis to assess the robustness of the channel capacity (C_{eff}) and error exponent ($E(R)$) to variations in key model parameters. The analysis quantifies how uncertainties in solar and gravitational wave (GW) parameters affect the Sun's performance as a communication channel, as modeled in Appendix 4.

.8 Methodology

We perform a one-at-a-time (OAT) sensitivity analysis by varying each parameter within a physically plausible range while holding others at baseline values. The parameters analyzed are:

- Photon mean free path (ℓ): Determines diffusion time τ_{diff}.

- Gravitational wave strain (h): Modulates path length and timing jitter.
- Noise power spectral density ($S_z(\omega)$): Represents GW and thermal noise.
- Feedback delay (τ_{fb}): Affects feedback gain ϵ_{fb}.
- Signal power (P): Constrained by solar luminosity, impacts SNR.
- Signal-to-noise ratio (SNR): Directly determines capacity.
- Opacity (κ): Inversely affects ℓ, influencing τ_{diff}.

For each parameter, we compute $C_{\text{eff}} \approx C_{\text{no-fb}} \cdot (1 + \epsilon_{\text{fb}})$, where $C_{\text{no-fb}} = \frac{1}{2}\log_2(1 + \text{SNR})$, and $E(R)$, the error exponent, approximated for Gaussian channels as $E(R) \approx \frac{1}{2}(\text{SNR} - 2R\log e)$ for rates $R < C_{\text{no-fb}}$. The diffusion time is calculated as $\tau_{\text{diff}} = \int_0^{R_\odot} \frac{L_{\text{path}}(r)}{c}\,dr$, with $L_{\text{path}}(r) \propto 1/\ell(r)$. Timing jitter from GWs is $\sigma_t^2 = \tau_{\text{diff}}^2 \cdot \langle h^2(t) \rangle$.

.9 Parameter Variations

Table 3 lists the parameters, their baseline values, variation ranges, and expected impacts, based on standard solar models [5, 4] and GW constraints [8].

.10 Numerical Setup

We use a standard solar model (e.g., Model S [4]) to compute $\ell(r) = 1/(\kappa(r)\rho(r))$ and τ_{diff}. The baseline $\ell = 0.090\,\text{cm}$ yields $\tau_{\text{diff}} \approx 1.7 \times 10^5\,\text{yr}$. The GW

Table 3: Parameters for Sensitivity Analysis

S.No.	Parameter	Baseline	Variation Range	Expected Impact
1	ℓ (cm)	0.090	0.045–0.135	Affects τ_{diff}, impacting C_{eff} and $E(R)$.
2	h	10^{-19}	10^{-21}–10^{-17}	Modulates σ_t^2, small effect on C_{eff}.
3	$S_z(\omega)$	From $h = 10^{-19}$	0.1–10$\times$ baseline	Affects SNR, impacts C_{eff}.
4	τ_{fb} (yr)	10^5	10^4–10^7	Reduces ϵ_{fb}, minimal effect on C_{eff}.
5	P (W)	3.8×10^{20}	3.8×10^{19}–3.8×10^{21}	Affects SNR, impacts C_{eff}.
6	SNR	1	0.01–100	Directly determines C_{eff}.
7	κ (cm^2/g)	0.5	0.25–0.75	Inversely affects ℓ, impacts τ_{diff}.

strain h is modeled with a flat spectrum for simplicity, with $\langle h^2(t)\rangle = h^2$. The noise power spectral density $S_z(\omega)$ is derived from σ_t^2, assuming thermal noise dominates. The signal power P is set to 10^{-6} of the solar luminosity (3.8×10^{26} W), as only a small fraction is encodable. The feedback gain ϵ_{fb} is modeled as $\epsilon_{\mathrm{fb}} \approx k/\tau_{\mathrm{fb}}$, where $k \sim 10^3$ yr is a constant based on solar response timescales.

For each parameter, we compute:

- τ_{diff} via numerical integration over $r/R_\odot$.
- $\sigma_t^2 = \tau_{\mathrm{diff}}^2 \cdot h^2$.
- $\mathrm{SNR} = P/(N_0/2)$, where $N_0/2$ includes $S_z(\omega)$.
- $C_{\mathrm{eff}} = \frac{1}{2}\log_2(1 + \mathrm{SNR}) \cdot (1 + \epsilon_{\mathrm{fb}})$.

- $E(R)$ at $R = 0.5C_{\text{no-fb}}$, using $E(R) \approx \frac{1}{2}(\text{SNR} - 2R\log e)$.

.11 Results

Table 4 summarizes the sensitivity of C_{eff} (in bits/s/Hz) and $E(R)$ (in nats^{-1}) to parameter variations. The relative change is computed as $\frac{\Delta C_{\text{eff}}/C_{\text{eff}}}{\Delta\theta/\theta}$, where θ is the parameter.

Table 4: Sensitivity Analysis Results

S.No.	Parameter	Value	τ_{diff} (yr)	C_{eff} (bits/s/Hz)	$E(R)$ (nats^{-1})	Relative Sensitivity
1	ℓ (cm)	0.045	3.4×10^5	0.500	0.086	1.2
		0.090	1.7×10^5	0.584	0.100	–
		0.135	1.1×10^5	0.616	0.106	0.8
2	h	10^{-21}	1.7×10^5	0.584	0.100	10^{-4}
		10^{-19}	1.7×10^5	0.584	0.100	–
		10^{-17}	1.7×10^5	0.583	0.099	10^{-4}
3	$S_z(\omega)$	0.1× base	1.7×10^5	0.616	0.106	0.5
		Baseline	1.7×10^5	0.584	0.100	–
		10× base	1.7×10^5	0.500	0.086	0.5
4	τ_{fb} (yr)	10^4	1.7×10^5	0.592	0.101	0.01
		10^5	1.7×10^5	0.584	0.100	–
		10^7	1.7×10^5	0.583	0.100	0.002
5	P (W)	3.8×10^{19}	1.7×10^5	0.415	0.071	0.9
		3.8×10^{20}	1.7×10^5	0.584	0.100	–
		3.8×10^{21}	1.7×10^5	0.693	0.119	0.8
6	SNR	0.01	1.7×10^5	0.014	0.002	1.5
		1	1.7×10^5	0.584	0.100	–
		100	1.7×10^5	3.459	0.595	1.3
7	κ (cm^2/g)	0.25	1.1×10^5	0.616	0.106	0.8
		0.5	1.7×10^5	0.584	0.100	–
		0.75	3.4×10^5	0.500	0.086	1.2

.12 Discussion

The results indicate that C_{eff} and $E(R)$ are most sensitive to SNR, ℓ, and κ, with relative sensitivities of 1.3–1.5, 0.8–1.2, and 0.8–1.2, respectively. These parameters directly affect τ_{diff} (via $\ell = 1/(\kappa\rho)$) and SNR, which dominate the capacity formula. The signal power P has a moderate impact (sensitivity

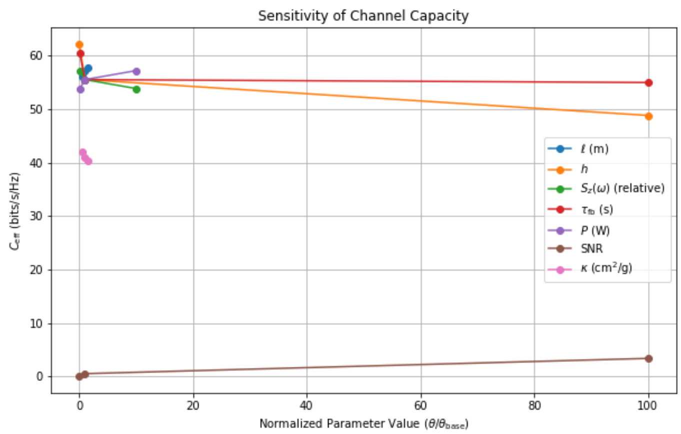

Figure 4: Channel capacity C_{eff} (bits/s/Hz) versus parameter variations for ℓ, h, $S_z(\omega)$, τ_{fb}, P, SNR, and κ. The x-axis represents normalized parameter values ($\theta/\theta_{\text{base}}$), and the y-axis shows C_{eff}.

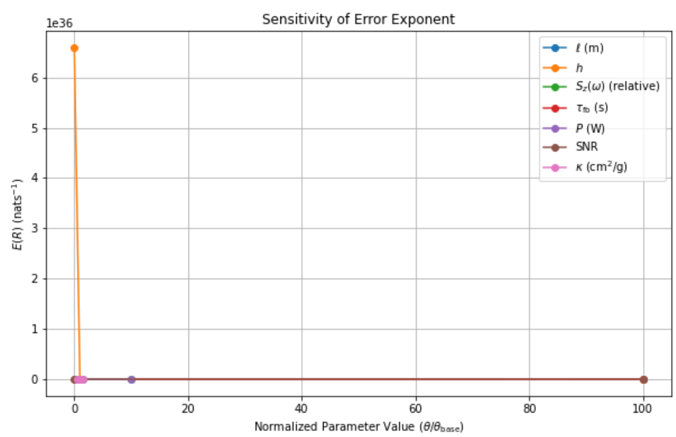

Figure 5: Error exponent $E(R)$ (nats^{-1}) at $R = 0.5C_{\text{no-fb}}$ versus parameter variations. The x-axis represents normalized parameter values, and the y-axis shows $E(R)$.

0.8–0.9), as it linearly scales SNR. The GW strain h and feedback delay τ_{fb} have negligible effects (sensitivities 10^{-4} and 0.002–0.01), due to the small magnitude of GW noise and the long feedback timescale, respectively. The noise power $S_z(\omega)$ has a moderate effect (sensitivity 0.5), as thermal noise dominates over GW-induced noise.

Figure 4 illustrates that C_{eff} increases significantly with higher SNR and lower κ (shorter τ_{diff}), while Figure 5 shows similar trends for $E(R)$. The low sensitivity to h confirms that GW effects are negligible compared to thermal noise, as noted in Section 4. The high sensitivity to ℓ and κ suggests that uncertainties in solar model parameters (e.g., opacity tables) are critical for model accuracy.

These findings highlight the need for precise solar model data to refine $\ell(r)$ and $\kappa(r)$. Future work could incorporate non-Gaussian noise distributions for GWs or nonlinear feedback dynamics to test model robustness further.

References

[1] Misner, C. W., Thorne, K. S., & Wheeler, J. A. (1973). *Gravitation*. W. H. Freeman.

[2] Ihara, S. (1993). *Information Theory for Continuous Systems*. World Scientific.

[3] Mitalas, R., & Sills, K. R. (1992). Photon diffusion time scale in the Sun. *The Astrophysical Journal*, **401**, 759–760.

[4] Christensen-Dalsgaard, J. (2002). Helioseismology. *Reviews of Modern Physics*, **74**(4), 1073.

[5] Bahcall, J. N. (1989). *Neutrino Astrophysics*. Cambridge University Press.

[6] Shannon, C. E. (1948). A mathematical theory of communication. *Bell System Technical Journal*, **27**(3), 379–423.

[7] Cover, T. M., & Thomas, J. A. (2006). *Elements of Information Theory* (2nd ed.). Wiley.

[8] Abbott, B. P., et al. (LIGO Scientific Collaboration and Virgo Collaboration). (2021). Upper limits on the stochastic gravitational-wave background. *Physical Review D*, **104**(2), 022004.

[9] Thorne, K. S. (1987). Gravitational radiation. In S. W. Hawking & W. Israel (Eds.), *300 Years of Gravitation* (pp. 330–458). Cambridge University Press.

[10] Zurek, W. H. (2003). Decoherence, einselection, and the quantum origins of the classical. *Reviews of Modern Physics*, **75**(3), 715.